Preprint Cambridge Centre for Computational Chemical Engineering ISSN 1473 – 4273

The sun always shines somewhere. The energetic feasibility of a global grid with 100% renewable electricity

Frederick Ivens[1], Jethro Akroyd[1,2], Markus Kraft[1,2,3]

released: February 14, 2025

[1] Department of Chemical Engineering
and Biotechnology
University of Cambridge
Philippa Fawcett Drive
Cambridge, CB3 0AS
United Kingdom

[2] CARES
Cambridge Centre for Advanced
Research and Education in Singapore
1 Create Way
CREATE Tower, #05-05
Singapore, 138602

[3] Department of Chemical Engineering
Massachusetts Institute of Technology
77 Massachusetts Avenue, Room 66-350
Cambridge, Massachusetts 02139

Preprint No. 334

UNIVERSITY OF CAMBRIDGE

Keywords: Global electricity grid, High-voltage direct current, Renewable electricity systems, Inter-continental transmission

Edited by
Computational Modelling Group
Department of Chemical Engineering and Biotechnology
University of Cambridge
Philippa Fawcett Drive
Cambridge, CB3 0AS
United Kingdom

E-Mail: mk306@cam.ac.uk
World Wide Web: https://como.ceb.cam.ac.uk/

Abstract

The defossilisation of the global electricity system is critical for mitigating climate change. Wind and solar PV play critical roles in this shift; however, their intermittency presents a significant challenge. Intercontinental electricity transmission offers a potential solution to mitigate this intermittency. This study investigates the energetic feasibility of a global electricity grid solely relying on wind and solar PV energy at a much higher spatial resolution of renewable potentials than in previous studies of global grids. The simulations suggest that a global grid could reduce excess electricity generation by up to 92% compared to an equivalent no transmission scenario and increase the correlation coefficient between the time-varying global generation and demand to 0.65. Analysis of global power flows estimated that approximately 3.6% of global demand would be lost during transmission. The study contextualised the power lost through transmission and curtailment by comparing it to the losses that would occur if other energy vectors (*e.g.*, hydrogen) were used or if the curtailed power were redirected for other purposes. The efficiency of the global grid was found to be significantly higher than that of hydrogen – 93.1% compared to approximately 30%. Additionally, if the excess electricity were used for hydrogen production, direct air capture (DAC), or desalination, it could address approximately 21.1% of the anticipated global hydrogen demand in 2050, 3.3% of the global CO_2 removal required by 2030 to meet Net Zero targets, or meet 33% of the estimated global freshwater demand in 2050 through desalination.

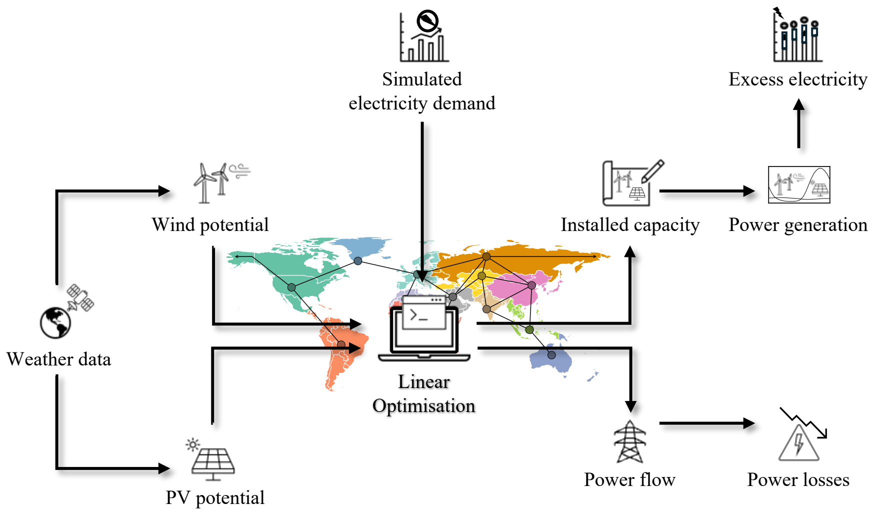

Highlights

- Optimising a global renewable electricity system to minimise surplus generation.
- Spatial allocation of wind and solar PV deployment and inter-regional power flow simulation.
- Time-series analysis of global power flows, regional generation, and demand profiles.

Contents

1 Introduction

So far, economic growth has heavily relied on fossil fuel combustion, leading to significant greenhouse gas emissions. It is indisputable that these emissions must be drastically reduced to avoid the worst effects of climate change. According to the United Nations Climate Action group, "Transitioning to a net-zero world is one of the greatest challenges humankind has faced" [28]. Among the major contributors to these emissions is the energy sector, which is responsible for two-thirds of global CO_2e emissions, with 40% stemming from electricity production. Currently, only 29.6% of electricity comes from renewable sources – a share that urgently needs to increase [19].

Renewable energy sources can be categorised into dispatchable and variable (V-RES) sources. Dispatchable sources, such as hydropower, biomass, geothermal, and concentrated solar power plants with thermal storage, have controllable outputs. In contrast, V-RES, such as wind and solar PV, are intermittent and dependent on environmental conditions. One of the major challenges of relying solely on variable renewable energy sources is the mismatch between generation and demand patterns, since temporal fluctuations of renewable potential depend on weather patterns which do not correlate with the electricity demand patterns. Interconnecting variable renewable energy sources across different geographic locations, that experience diverse weather patterns, has been proposed as a solution to mitigate these fluctuations.

Ultra-high voltage transmission technologies enable the transmission of electricity over long distances with losses of 2–4% per 1,000 km, facilitating the connection of electricity grids across continents [33]. The European Union plans to connect solar and wind farms in Egypt to the European mainland [12]. Singapore is constructing an interconnector to Australia to supply up to 15% of its electricity demand [5], and the UK and Morocco have plans to link large-scale solar and wind farms in Morocco to the UK's electricity grid [32]. Theoretically, this concept could be expanded globally. While wind and solar are intermittent on a regional scale, they are less intermittent globally; the sun always shines somewhere, and the wind always blows somewhere. A global electricity grid could transmit electricity generated from renewable sources from surplus regions to deficit regions, smoothing supply and demand.

In recent years, the development of energy system models to assess the benefits of intercontinental energy interconnections has garnered significant attention. Extensive research has explored these systems on an intercontinental scale, though not globally, including studies by Ardelean [2], Ardelean and Minnebo [3], Bogdanov and Breyer [7], Brown and Botterud [9], Purvins et al. [23], Reichenberg et al. [24], Zappa et al. [34]. In contrast, global electricity grids have been investigated by Yu et al. [33] and Wu et al. [31]. Yu et al. [33] conducted a feasibility study of a global electricity grid with 20 interconnections across 13 regions, aiming to identify the optimal mix of generation technologies that would minimize costs while meeting global electricity demand in 2050. Wu et al. [31] focused on the economic benefits of a global grid powered entirely by renewable energy by 2050. Their study modeled 20 potential interconnection routes across 14 regions, exploring various scenarios, including those limited to variable renewable energy sources.

A key limitation of these studies is their averaging of renewable energy potential across entire regions. One of the primary motivations behind a global grid is to create a generation profile that aligns more closely with the demand curve. This can be achieved by combining generation potentials from different regions, each driven by distinct weather patterns that act as independent variables. Averaging wind and solar potentials over large regions risks losing important intra-regional weather variability and thus limit the ability to match global electricity demand effectively.

The **purpose of this paper** is to address this limitation by investigating the energetic feasibility of a global electricity grid that is solely powered by wind and solar PV energy, and does not rely on energy storage. A key improvement is the use of a much higher spatial resolution for renewable potential profiles compared to earlier studies of global grids. To achieve this, we developed a computational model of a global electricity grid in PyPSA. This model uses linear optimisation to determine the regional deployment of wind and solar PV capacities that minimise excess electricity generation. It also simulates power flows between regions, considering both regional electricity demand and renewable energy potential profiles at an hourly resolution for an entire year. The renewable energy potential is modelled at a spatial resolution of $4° \times 4°$, significantly higher than the regional averages used in previous studies [31, 33]. For comparison, we also simulated a "no transmission" scenario, in which power flows between regions are restricted.

2 Method

Investigating the energetic feasibility of a global electricity grid powered entirely by wind and solar PV requires an understanding of several key things. Fundamentally, power flow in a global grid is driven by differences in electricity demand and supply. Electricity generation is a function of the installed wind and solar PV capacities in each region and the time-varying capacity factors. Therefore, to accurately simulate the behaviour of a global electricity grid over multiple time steps, time-varying electricity demand, installed wind and solar PV capacities, and time-varying capacity factors are required. While electricity demand can be predicted through various methods and capacity factors derived from weather data, the optimal spatial distribution of wind and solar PV capacities is to be determined. For this purpose, a computational model is needed that considers the time-varying electricity demand and the time-varying capacity factors of each region, and models power flow in the grid to spatially allocate wind and solar PV capacities.

Initially, a suitable grid architecture must be selected. An existing architecture was adapted from previous work. The grid architecture from Yu et al. [33] was used. It is displayed in **Figure 1**. An overview of the countries corresponding to the regions, the interconnector specifications and the coordinate reference system for each region are provided in Section A.1 of the Appendix.

Each region of the grid is characterised by its potential renewable energy generation profile and electricity demand profile, with the spatial and temporal resolution of these profiles determining the complexity and accuracy of the simulation. Historic weather data, from which the renewable potentials are derived, is available at an hourly resolution. This aligns with the objectives of this study, as the focus is on how the grid responds to fluctuations in supply and demand throughout the day and year, rather than on modelling control

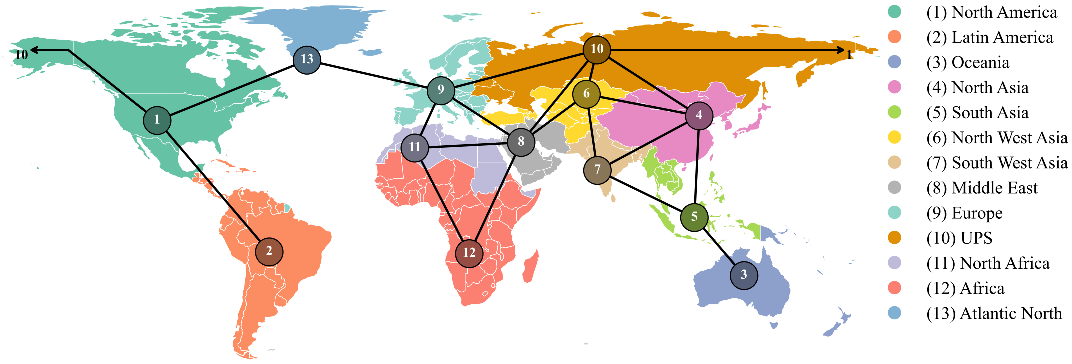

Figure 1: *Map of the global electricity grid used in this work. Adapted from CIGRE [33].*

problems at a timescale of seconds (which are assumed to be solvable). Therefore, the behaviour of the global grid is investigated at an hourly frequency. This study focuses on variable renewable energy sources, so a scenario where only wind and solar PV capacities are deployed is investigated, neglecting existing generation plants and potential energy storage.

2.1 Time series predictions of electricity demand

Annual electricity demand data is required for each region. Generally, it can be differentiated between historical data and synthetic data. Historical data refers to actual past electricity consumption, typically published by government agencies. In contrast, synthetic data is generated artificially, either through statistical and probabilistic models that simulate electricity consumption patterns or through machine learning models that predict electricity demand based on historical data and correlations with relevant factors such as weather, time of day, day of the week, and economic activity.

In this study, electricity demand time series predictions for regions around the world were obtained using synthetic data. For this purpose, the GlobalEnergyGIS model developed by Mattsson et al. [22] was utilised. It predicts full-year electricity demand series for 2015 at an hourly frequency. The 2015 demand series is then scaled via homothetic transformations to match estimates of annual country-level electricity demand in 2050, based on the SSP scenarios [25]. The model was trained on data from 44 countries using variables such as calendar effects, temperature variables, and economic indicators. The demand time series was projected to 2050 based on the SSP1-1.9 scenario. Details of the demand multipliers are given in Section A.2 of the Appendix. The code of the GlobalEnergyGIS model required slight modifications to fix bugs before it could be utilised. This version of the code is available via GitHub. See the code and data availability statement at the end of this manuscript.

2.2 Time series predictions of wind and solar energy potential

Wind and solar energy potential time series were predicted at an hourly frequency using historic meteorological re-analysis data. Unlike electricity demand, the wind and solar potential were not predicted for 2050 due to the uncertain future development. Instead, historic re-analysis data from 2023 was utilised.

Each region was subdivided into sub-regions, measuring $4^\circ \times 4^\circ$. For each of these sub-regions, a time series of wind and solar potential was predicted. For this, two things are required: (1) the hourly capacity factors; (2) the maximum deployable capacity. The product of the two is the hourly potential generation profile.

The hourly capacity factors are calculated using Atlite [18]. Initially, Atlite extracts and processes historic meteorological re-analysis data from the ERA5 database. For each ERA5 grid cell, Atlite calculates the wind and solar PV capacity factors. For wind, this is done by extrapolating the 10 m wind speeds to hub height of a defined turbine and evaluating its power curve. The Vestas V112 3 MW [6] turbine was chosen for reference due to its high power density. For solar PV, Atlite converts downward-shortwave and upward-shortwave radiation flux and ambient temperature into capacity factors for a defined panel at a specified orientation. Atlite's default solar panel (CSi) was chosen for reference, and the orientation is assumed to be optimal for any given latitude. For each sub-region, the spatial average of these capacity factors is calculated.

The maximum deployable capacity in each sub-region is the product of (a) the land area, (b) the installation density, and (c) the land-use availability. The land area for each sub-region was calculated using GeoPandas [14], with each region projected using an appropriate Coordinate Reference System (CRS) (see Section A.1 of the Appendix).

The installation densities were assumed to be 10 W/m^2 for wind and 45 W/m^2 for solar PV, and the land-use availabilities were assumed to be 8% for wind and 5% for solar PV [24, 31]. However, due to high uncertainties, the choice of these values was investigated as part of a sensitivity analysis. Offshore wind was excluded from this study.

2.3 Simulation of the global electricity grid

PyPSA was used to model and perform power flow analysis on the global grid. This section provides a comprehensive overview of how PyPSA was configured to optimise the spatial allocation of wind and solar capacities, aiming to minimise excess electricity generation.

PyPSA uses the time series of the electricity demand, the time series of the capacity factors, and the maximum potential installed wind and solar PV capacities at each node as input. It then computes the optimal solution – which aims to minimise excess electricity generation – for the network depicted in Figure 1. The optimal solution includes the following: (a) installed wind and solar capacities at each node; (b) time series of the wind and solar electricity generation at each node; (c) time series of the curtailed electricity at each node; (d) time series of the power flow between the nodes.

The components assigned to a node include (i) a wind and solar PV generator for the number of sub-regions within the region, (ii) a curtailment generator, (iii) a load, and (iv) one or more links.

To model intermittent behaviour accurately, the wind and solar generators must be configured accordingly. The power generated at any given time step is the product of the deployed capacity and the capacity factor at that time step. The deployed capacity, which is the decision variable during the optimisation, can vary between zero and its maximum value but remains constant across all time steps. Thus, the magnitude of electricity generated by a generator is controlled by its deployed capacity, while variations over time depend on the capacity factors.

The efficiency of the links between nodes was calculated based on the resistive losses. UHVDC cables were selected as transmission lines since UHVDC was identified as the preferred technology for intercontinental power transmission. Details of the power loss calculation and the technical properties of the UHVDC cables are given in Section A.3 of the Appendix. Additionally, losses of 1.5% were assumed for each converter pair – required when converting direct current (DC) to alternating current (AC) and vice versa. The lengths of the links were determined based on the geodesic distance between the nodes using the Python library *pyproj* [30].

PyPSA creates an economic model of the energy system. Although the economics of the global grid are not within the scope of this study, costs assigned to decision variables represent weights in the objective function and can therefore be considered relative to each other. The costs considered in this study include the cost of deployed capacity (per MW), the cost of power generated (per MWh), and the cost of power transmitted (per MWh). No costs were assigned to curtailment since the optimal solution will naturally minimise curtailment. Additionally, assigning costs to curtailment would incentivise the system to transmit electricity to other nodes to avoid curtailment, promoting undesirable behaviour.

The assignment of cost was investigated as part of a sensitivity analysis, which is further described in Section 2.4. Wind and solar were assigned equal costs since the objective is to minimise curtailment and if lower costs were assigned to solar, excess electricity from that source would be penalised less, leading to more excess generation compared to a configuration with equal penalisation. The costs were structured with a 1:1 (MWh/MW) ratio between the cost of deployed capacity and power generated, and a 10000:1 (MWh/MWh) ratio between the cost of power generated and electricity transmitted.

2.4 Sensitivity analysis

2.4.1 Parameter choice

A sensitivity analysis was performed to assess the sensitivity of the model to variations in the costs assigned to the decision variables and land-use availability. Specifically, the sensitivity of the model to:

- Capital costs compared to operational costs;
- Costs of wind compared to costs of solar;

- Costs of generation compared to costs of transmission;
- Variation in land-use availability.

The analysis focused on the impact on annual global generation, the share of wind and solar, and annual global transmission. Additionally, the impact on the power flow into North Asia was investigated.

2.4.2 Spatial resolution of renewable potential

A series of simulations were conducted where the resolution of the renewable energy potential was progressively increased up to a maximum resolution of 2°×2° to investigate the influence of the spatial resolution of the renewable potential on the performance of the global grid, and confirm the convergence of the results that are presented in what follows.

3 Discussion

The results discussed in this section reflect the outcomes from the 4°×4° transmission scenario.

3.1 Analysis of global grid performance

In this simulation, electricity generation and transmission are driven by electricity demand. The projected global electricity demand in 2050 is 54,000 TWh. As shown in **Figure 2**, North Asia is expected to account for 39.6% of this demand. North America follows with 14.9%, and South West Asia and the Middle East each account for 8.5%.

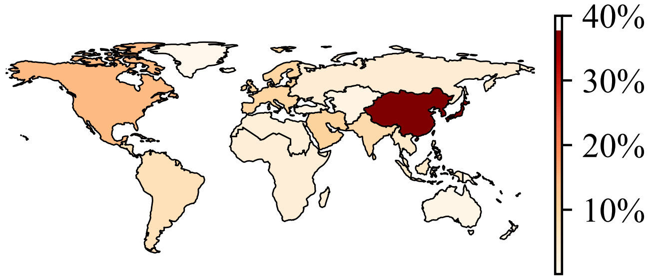

Figure 2: *Annual electricity demand in 2050 for each region as a share of global electricity demand.*

Figure 3 shows that in the no transmission scenario, where each region must produce its own electricity, a total of 115,500 TWh needed to be generated to consistently meet demand. This scenario results in an annual excess electricity generation of 61,500 TWh. Conversely, in the transmission scenario, these figures are reduced to 60,900 TWh of required generation and 4,940 TWh of excess generation, representing an 92% reduction in excess generation.

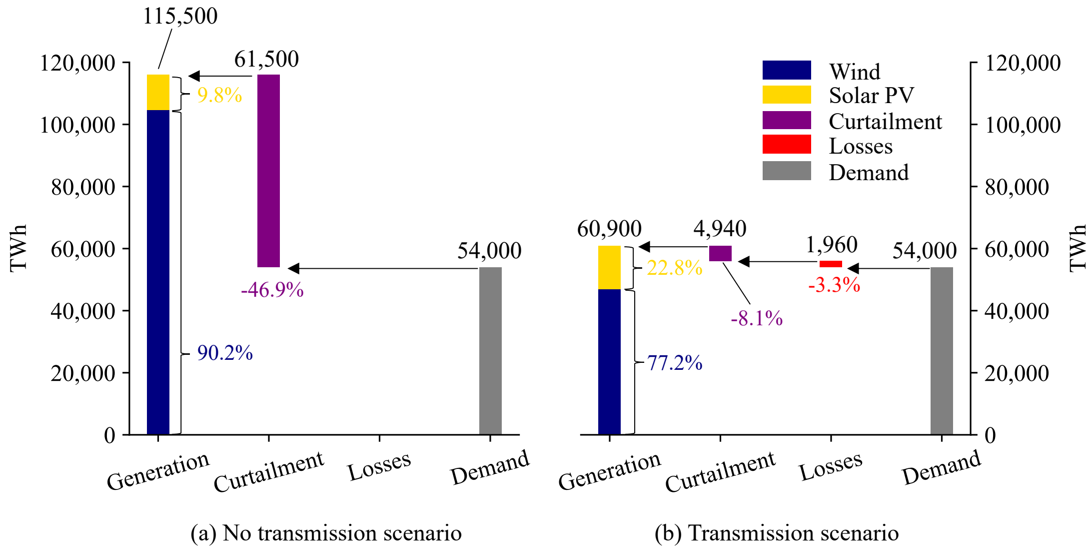

Figure 3: *Comparison of annual global generation, curtailment, transmission, and demand in the (a) no transmission scenario and (b) transmission scenario.*

3.1.1 Global power flow

A global electricity grid mitigates curtailment by enabling transmission between regions. This allows regions with a surplus to supply those with a deficit, balancing demand and supply. **Figure 4** illustrates the annual net flows via the links between regions in the model, highlighting significant variations in their utilisation.

The largest flows are observed into or out of North Asia, North West Asia, North America, Oceania, South Asia, Europe, and UPS, while Africa, Latin America, and Atlantic

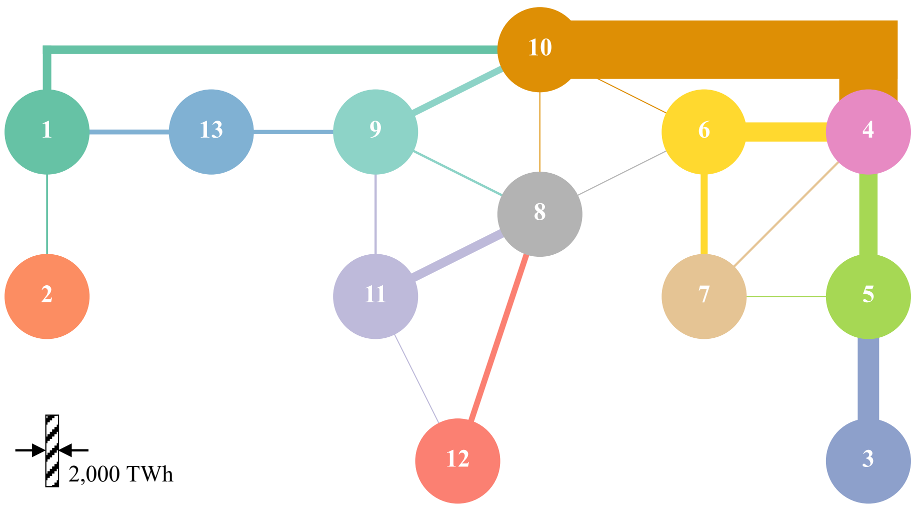

Figure 4: *Annual net flows of power between the nodes of the global grid in 2050. The numbers in the nodes have the same meaning as in Figure 1. The width of the lines is proportional to the power flow.*

North experience relatively small flows. In total, an annual power flow of 28,900 TWh is observed, representing 47.3% of annual generation. However, this figure can be misleading, as power may flow through multiple links, leading to the possibility of double counting. A more accurate measure considers only the actual net outflows from nodes, which represents the true share of generated electricity being transmitted. Based on this, total net outflows accumulate to 19,500 TWh, representing 32.1% of global generation, meaning that one-third of the global electricity demand is supplied by electricity imports.

Notably, the majority of flows are directed towards North Asia. Although North Asia accounts for approximately 37.5% of global demand, it receives over 90% of global annual net flows. Even non-neighbouring regions contribute to North Asia's electricity supply through intermediary regions. For instance, electricity generated in North America passes through the UPS to reach North Asia, despite an 18% efficiency loss along this route.

Figure 5 shows the underlying reason for this behaviour. North Asia has an annual electricity demand of 20,000 TWh but generates less than 6,500 TWh. Consequently, it imports more than two-thirds of the electricity it consumes, which equates to nearly one-quarter of global demand. To meet this demand, some regions generate significantly more electricity than they consume. Atlantic North generates 79 times its annual electricity demand, Oceania 11 times, and Africa 2 times its annual demand. However, these regions also curtail a significant portion of their excess electricity: Atlantic North curtails 32% of its generated electricity, while Oceania and Africa curtail 20% and 30%, respectively. In contrast, UPS and North West Asia, which generate 5 and 6 times their annual electricity demand, curtail significantly less – 3% and almost none, respectively.

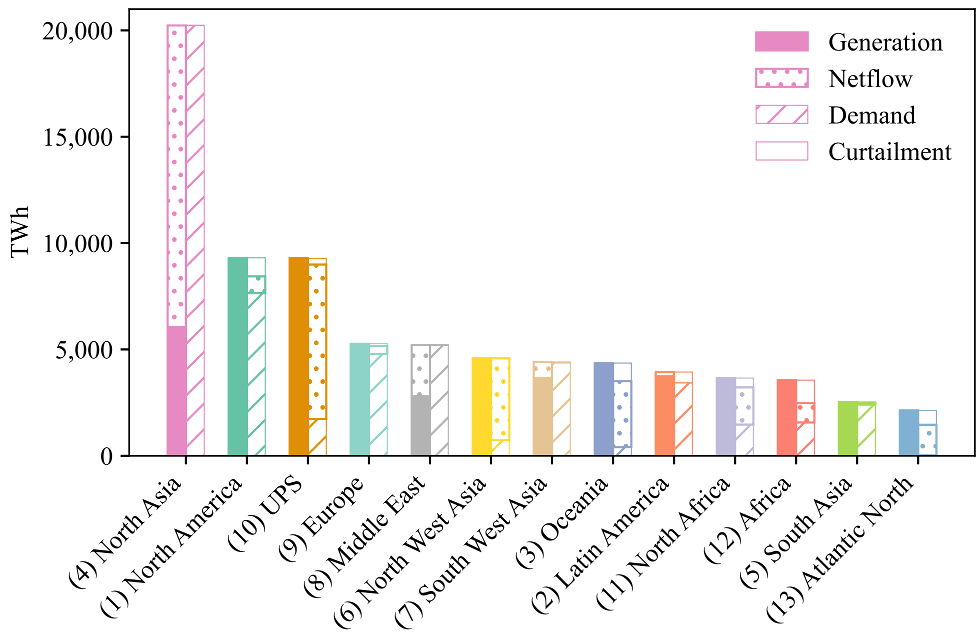

Figure 5: *Regional annual generation, demand, curtailment, and net flow in 2050. Inflows are in the left column and outflows in the right column.*

3.1.2 Node categorisation

Figure 6 visualises the behaviour of regions concerning annual generation, demand, curtailment, and inflow and outflow. The nodes are categorised as net importers, net exporters, or hubs. Net importers are defined as nodes that import at least one-third more electricity than they export. Conversely, net exporters are nodes that export at least one-third more electricity than they import. Hubs are nodes where the inflow and outflow values are within a one-third tolerance of each other, indicating the majority of electricity is simply passing through.

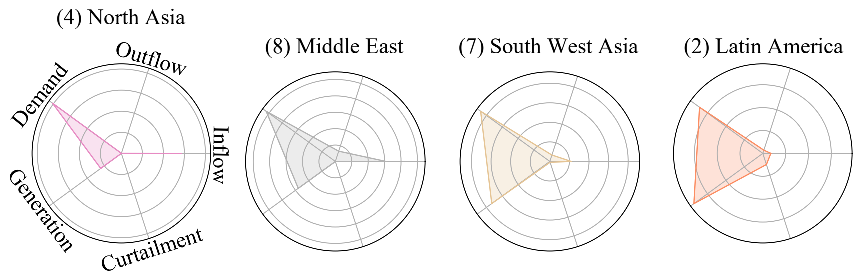

(a) Net importers. Nodes that import one-third more than they export.

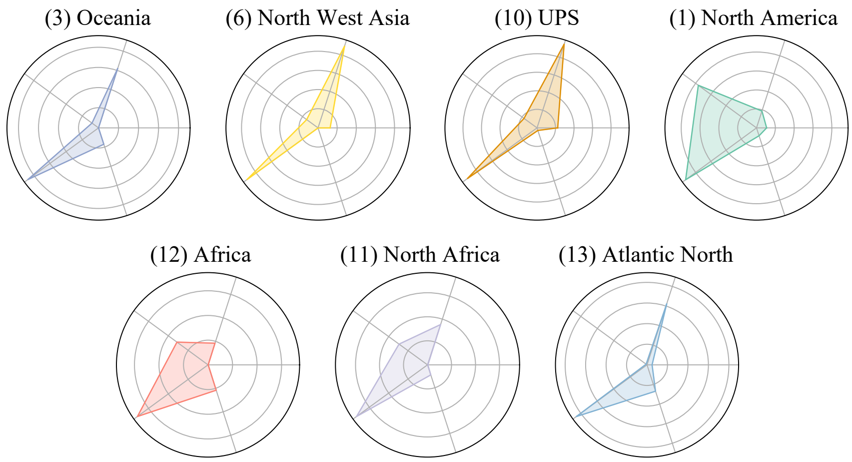

(b) Net exporters. Nodes that export one-third more than they import.

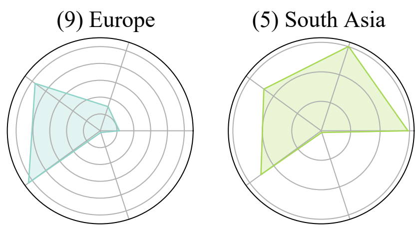

(c) Hubs. Nodes that exhibit both inflow and outflow values within a one-third tolerance of each other.

Figure 6: *Categorisation of nodes depending on whether they act as net importers, net exporters or hubs. The radar charts are on different radial scales.*

Figure 6 shows that four nodes act as net importers, seven as net exporters, and two as hubs. Among the net importers, North Asia imports 70% of its demand, Middle East 59%, South West Asia 25%, and Latin America 10%. Notably, North Asia, South West Asia, and Middle East barely curtail any electricity, indicating that these regions either frequently exhibit a generation deficit or effectively manage to export surplus electricity. On the other hand, Latin America curtails 13.7% of the electricity it generates. For reference, in 2020, England and Wales curtailed only 0.5% of their generated wind energy, while Scotland curtailed up to 20% [4], illustrating that significant differences in curtailment rates are observed in actual energy systems as well.

Among the net exporters, Oceania is the only region that does not import any electricity at all, thus, it constantly exhibits an electricity surplus. Three of the seven regions – Oceania, North Africa, and Africa – export more than 100 times what they import. The remaining four regions – Atlantic North, North West Asia, UPS, and North America – export approximately 13 times, 7 times, 4 times, and 2 times of what they import. These observations suggest that the net exporters generate electricity to supply other regions.

3.1.3 Time series analysis

The behaviour of the regions can be better understood through a time series analysis of the corresponding demand and generation profiles. Fundamentally, a region needs to import electricity when the generation-to-demand ratio is less than one. If this ratio exceeds one, the region has an electricity surplus and must either export or curtail the excess electricity. The optimal ratio is one, where supply matches demand.

Figure 7 shows the generation-to-demand profiles for two selected regions. It can be observed that North Asia experiences a demand deficit in 8,754 hours (99.9%) of the year, whereas UPS does not experience a deficit at all. Unlike UPS, which minimises curtailment by exporting surplus electricity, North Asia is minimising curtailment by deploying just enough capacity to meet the minimum demand. The Middle East exhibits a very similar behaviour to North Asia, experiencing a demand deficit 97.8% of the time.

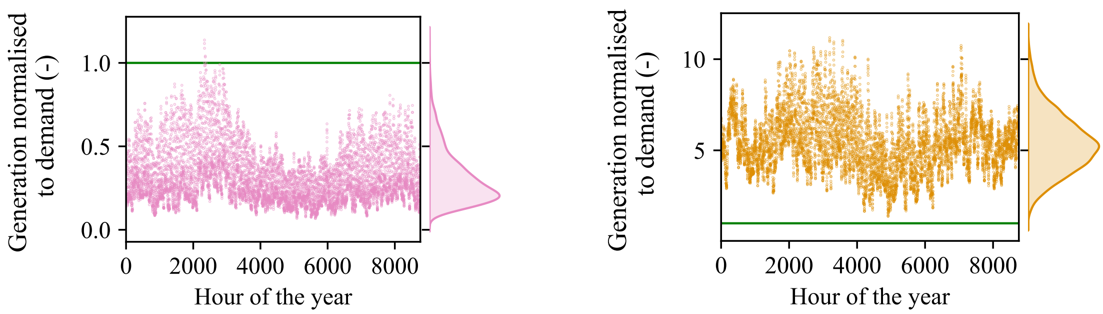

(a) North Asia.

(b) UPS.

Figure 7: *Annual generation of (a) North Asia and (b) UPS normalised to demand for the year 2050. Each dot represents the generation-to-demand ratio for one hour of the year.*

The generation-to-demand ratio was computed for every region at each time step. The aggregated behaviour across regions was such that net importers were observed to exhibit an electricity deficit 77.4% of the time, compared to net exporters which exhibited a surplus 87.6% of the time. The profiles are available in Section A.4 (Figure A.1) in the Appendix.

Previously, it was outlined that Latin America curtails 13.7% of the electricity it generates. Latin America's generation-to-demand profile reveals that it experiences an electricity deficit only 43% of the time. Thus, it exhibits a surplus more frequently than a deficit, which initially suggests it might be a net exporter. However, exports from Latin America occur in only 30% of the hours it has a surplus; in the remaining hours, it curtails the excess electricity. It is hypothesised that the time series of their electricity surplus do not align well with the needs of other nodes or that the transmission losses are less favourable than alternatives which would indicate that surplus electricity alone is not sufficient for exports; there must also be a corresponding demand at this time step. Another noteworthy observation is that South Asia and Europe primarily function as transit nodes. Despite experiencing a demand deficit 57% and 49% of the time, they export electricity 82% and 62% of the time, respectively, indicating that electricity imported from other nodes is often re-exported even during periods of deficit.

These observations highlight that, while a clear distinction between net importers and net exporters can be made, the underlying patterns in these regions vary significantly. To investigate why some nodes act as net importers and others act as net exporters, it is essential to recall the aim of the optimisation. The aim is to allocate wind and solar capacity to satisfy demand at minimal cost, *i.e.*, minimal excess electricity generation. Considering this, one can look at the regional cost of electricity in terms of the amount of electricity that had to be curtailed to generate one useful unit of electricity. For the no transmission scenario, this is straightforward. Since each region consumes only the electricity it generates, the curtailed electricity can be unambiguously mapped to a region. It can be observed that the cost of electricity does not vary much between the regions, as is to be expected due to the variable nature of wind and solar energy.

For the transmission scenario, this is more complex. While the curtailed electricity is known for each region, the cause of the curtailment cannot be unambiguously mapped to a single region. Nevertheless, it is believed that, when looking at a single time step, a deficit in one region is supplied by the region that has the least curtailment (due to the extra capacity that had to be installed to supply this time step) at the other time steps. This implies that regions capable of minimising curtailment across multiple time steps (when supplying electricity to other regions) are likely to act as suppliers. It is hypothesised that regions with renewable generation profiles that best align with the electricity demand profiles of the receiving regions are better positioned to minimise curtailment and thus act as suppliers. This could explain why North Asia acts as the main importer, as its demand deficit profile might align well with the renewable potential profiles of the exporting regions. However, a regression analysis, in which the independent variables were the wind and solar capacity factors of two regions and the dependent variable was the sum of their electricity demand profiles, did not yield significant insights. The correlation matrix is available in Section A.4 (Figure A.2) in the Appendix.

Figure 8 illustrates the global generation curve alongside the global demand curve in both the no transmission and transmission scenarios. In the introduction, it was highlighted that one of the primary motivations for a global electricity grid is to create a generation profile that aligns more closely with the demand curve. It can be observed that in the transmission scenario, the seasonal trends present in the demand profile are more closely mirrored compared to the no transmission scenario. This improvement can be quantified by calculating the Pearson correlation coefficient between the global generation and demand profiles in both scenarios. In the no transmission scenario, the correlation coefficient is 0.09, indicating a weak alignment between generation and demand. However, in the transmission scenario, the correlation increases to 0.65, demonstrating that the global grid effectively increases the number of independent variables available to the system. This enhanced flexibility enables the system to better assimilate the demand curve, improving the performance of an electricity system powered entirely by variable renewable energy sources.

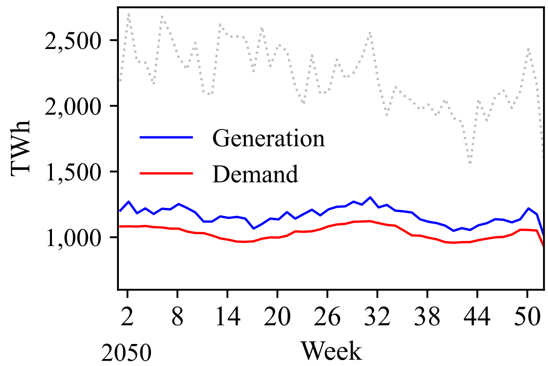

Figure 8: *Global weekly energy demand and generation profiles of the transmission scenario, with the no transmission scenario shown for reference as the dotted line.*

3.1.4 Frequency analysis

To investigate temporal patterns in the power flow of the global grid, a frequency analysis of the net flow into and out of regions was conducted. The analysis identified events with 6-hour, 8-hour, 12-hour, and daily frequencies, with considerable variation in the strength of these effects across different regions.

Strong daily patterns, where daily fluctuations around the mean are larger than the mean, are observed in North America, Latin America, and Europe. In the remaining regions, only weak daily patterns can be observed. **Figure 9** shows sample spectra. The spectra for all regions are available in Section A.4 (Figure A.3) in the Appendix.

It is hypothesised that the solar cycle is a primary cause of the daily frequency. However, on average, regions exhibiting strong daily patterns do not exhibit higher shares of solar PV than the remaining regions so that this hypothesis is hard to confirm. The other frequencies are much less pronounced than the daily frequency. Potential causes for these frequencies include the day-night transition (12-hour frequency), the human workday (8-hour frequency), and diurnal wind patterns (6-hour frequency).

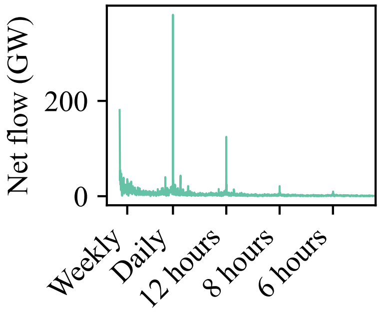

(a) Strong daily pattern.

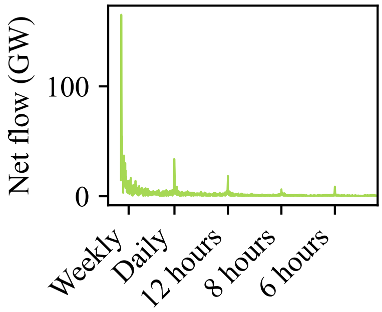

(b) Weak daily pattern.

Figure 9: *Fourier transform of the hourly net flow through a region that experiences (a) a strong daily pattern – North America and (b) a weak daily pattern – South Asia. Each panel uses its own scale for the net flow axis.*

3.2 System efficiency

So far, a comprehensive overview of the dynamics of the global grid has been provided, focusing on spatial generation, spatial curtailment, and power flow between regions, along with a detailed analysis of the role of individual regions within the grid. However, the grid's efficiency has not yet been examined. This section offers a detailed overview of transmission losses and curtailment.

Figure 10 summarises the hourly relative losses and curtailment. The losses range from a minimum of 1.0% to a maximum of 7.2%, with a mean of 3.6% relative to demand lost in transmission, indicating that there is always a certain threshold of electricity transmitted between the regions. On average, 7.9% of the global electricity generated is curtailed.

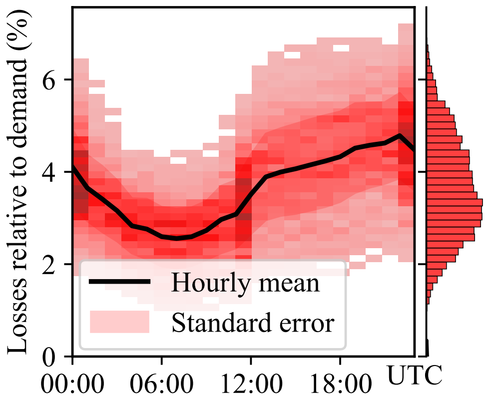

(a) Relative losses.

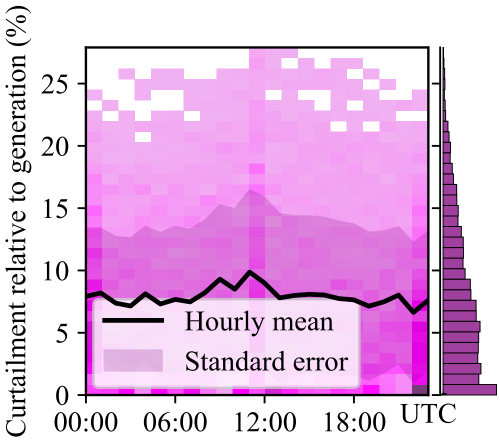

(b) Relative curtailment.

Figure 10: *Heat map, mean, standard error and frequency distribution of mean hourly global relative losses and curtailment against UTC in 2050. The losses are relative to the energy demand and curtailment is relative to generation.*

However, curtailment is entirely absent when the grid is perfectly balanced, but it can reach 27.9% of the generation, equivalent to twice the global electricity demand.

Losses relative to transmission range between 5.9% and 8.7%, with a mean of 6.9%. This range is narrower, and the mean is higher than when losses are calculated relative to demand because electricity can only be lost during transmission, whereas it is possible to meet demand without losses. Calculating losses relative to transmission sets the theoretical minimum to the efficiency of the shortest link, assuming that electricity is only transmitted along that link. Conversely, a "once-round" maximum loss would occur if electricity were transmitted only over the longest distance between two regions – such as between Oceania and Latin America, with an efficiency of 60% – though this scenario does not occur in the simulation.

3.3 Sensitivity analyses

Sensitivity analyses were performed to critically assess the behaviour of the transmission scenario. The key findings are summarised below.

3.3.1 Parameter choices

A sensitivity analysis was performed to examine the effect of the choice of nodal parameters. The most important findings are:

- Power flow decreases significantly when the cost of transmission exceeds the cost of generation. This is consistent with expectations, as the optimisation tends to favour generating additional energy at the demand node instead of transmitting already generated electricity.
- When the ratio between capacity cost and generation cost exceeds 100:1 MWh/MW, total generation begins to increase. This occurs because capacity costs penalise the deployment of capacity rather than electricity generation, shifting the focus away from minimising excess electricity generation. A solution might be preferred that deploys less capacity but generates more excess electricity overall.
- The ratio between the costs of wind and solar influences the generation mix. Higher solar costs result in a reduced share of solar in the generation mix, and vice versa.

Overall, the sensitivity analysis aligns with expected system behaviour, revealing that the simulation is largely insensitive to variations in parameters such as CapEx, OpEx, transmission costs, and land-use availabilities. The choice of parameters and the rational behind this choice as discussed in Section 2 has been shown to be reasonable. This finding is significant as it reduces uncertainties related to parameter selection and enhances the reproducibility of the study. Figures showing the impact of the parameter choice are available in Section A.5 of the Appendix.

3.3.2 Spatial resolution of renewable potential

A sensitivity analysis was performed to examine the effect of the resolution of renewable energy potentials on the behaviour of the global grid. As shown in **Figure 11**, the annual global electricity generation converges to approximately 60,000 TWh as the spatial resolution increases. Between resolutions of 8°×8° and 4°×4°, annual global generation decreases by 2.4%. However, the reduction diminishes with finer resolutions: from 4°×4° to 3°×3°, the difference is only 0.8%, and from 3°×3° to 2°×2°, it is only 0.2%. We consider the results at 4°×4° to be converged.

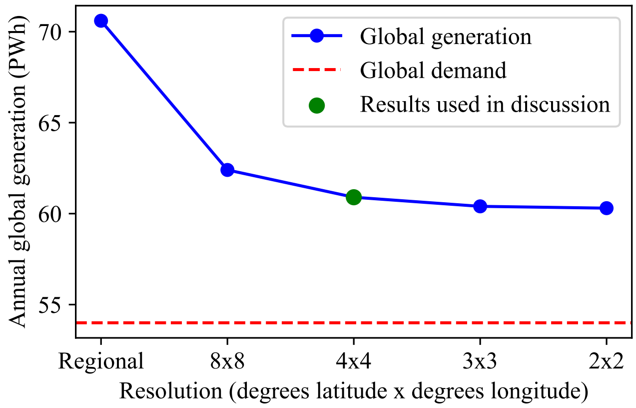

Figure 11: *Annual global electricity generation for different spatial resolutions of renewable potentials.*

The following changes in the generation profile were observed as the resolution was increased from regional to 4°×4°:

- The correlation coefficient between the global generation profile and the global demand profile increased from 0.08 in the regional scenario to 0.65 in the 4°×4° scenario.
- Curtailment was reduced by 72% in the 4°×4° scenario compared to the regional scenario.

Despite these improvements, the fundamental behaviour of the global grid remained largely independent of the resolution. North Asia continues to be the primary importer, receiving over 90% of power flows. While wind still accounts for three-quarters of global generation, the distribution of solar generation has become more balanced – only one region does not deploy any solar PV in the 4°×4° scenario, compared to six in the regional scenario. This shift could be attributed to the increased spatial resolution capturing more granular variations in the solar cycle within regions, thereby enabling more diverse generation patterns that involve solar PV.

3.4 Comparison to alternative energy carrier and future energy needs

This section seeks to understand the magnitude of power lost in transmission and curtailment in the context of losses that would be incurred if using other energy vectors, or if using the curtailed power for something else. An order of magnitude approach is taken.

3.4.1 Hydrogen and ammonia as alternative energy carriers

A global grid allows for the direct transmission of electricity from regions with a surplus to those with a deficit. An alternative to direct transmission is converting electricity into chemicals for transportation, with hydrogen and ammonia being frequently discussed options. In the latter process, electricity is first converted into hydrogen, then into ammonia, which is transported to the desired location and converted back to hydrogen for local consumption. However, significant energy losses occur during these conversion processes, with a round-trip efficiency of about 30% if the hydrogen is converted back to electricity using a fuel cell, meaning that 70% of the initial energy is lost [15]. When comparing this to the efficiency of the global grid, it makes sense to compare it to the losses relative to electricity transmission in the global grid since electricity is only converted for transport between regions. This efficiency averages 93.1% – significantly higher than the round-trip efficiency of hydrogen. While this helps put the efficiency of the grid into context, it should be noted that the analysis neglects the additional value that might be gained by using chemicals for energy storage, so care should be taken as and if building on this analysis in the future.

3.4.2 Installed capacity

To ensure the energetic feasibility of a global grid, a substantial amount of wind and solar PV capacity needs to be installed by 2050, with a greater emphasis on wind than solar PV. **Figure 12** illustrates this. Currently, Europe and Asia are the only regions that have installed a significant portion of the capacities predicted by the model. Europe has achieved approximately 10% of the predicted wind capacity and 15% of the predicted solar PV capacity. In contrast, Asia has installed 47% of the predicted solar PV capacity. However, it is important to note that this high percentage is a result of the simulation's spatial allocation of solar PV capacity, which assigned relatively little to Asia. This finding diverges from current global trends, particularly in 2023, when Asia – led by China – installed as much solar PV capacity as the rest of the world combined [20].

Globally, the model predicts that a total installed capacity of 54,301 GW for wind and 9,753 GW for solar PV would be needed. As of 2022, only 1.7% of the predicted wind and 10.8% of the predicted solar PV capacity has been installed, indicating a significant shortfall of 53,403 GW for wind and 8,700 GW for solar PV. To meet these hypothetical targets by 2050, an annual installation rate of more than 2,200 GW for wind and solar PV would be required. For reference, in 2023, 510 GW of renewable energy capacity were added globally [20].

3.4.3 Future energy needs

The model predicts that the global grid would generate 4,940 TWh of excess electricity annually. This represents a significant opportunity to address future energy needs. This section contextualises the potential use of excess electricity by comparing it to the energy needs of hydrogen production, direct air capture (DAC), and desalination of water.

Green hydrogen is produced via water electrolysis, which can be sub-categorised into low-temperature and high-temperature processes. Low-temperature electrolysis typically requires an energy input of 55–60 kWh per kilogram of hydrogen produced, while high-temperature electrolysis is more efficient, requiring approximately 40 kWh per kilogram of hydrogen [13]. Assuming the 4,940 TWh of excess electricity were utilised for high-temperature electrolysis, this could result in the production of 124 Mt of hydrogen annually. According to a McKinsey study, the projected global hydrogen demand in 2050, under a Net Zero scenario, is approximately 585 Mt [16]. Thus, the utilisation of global curtailed electricity for high-temperature electrolysis could potentially meet 21.1% of the anticipated hydrogen demand in 2050.

Direct air capture (DAC) using absorption and electrodialysis can remove CO_2 directly from the atmosphere using electricity. The electricity demand for DAC can vary significantly. Viebahn et al. [29] estimated that 1.89 MWh of electricity are required per tonne of CO_2 removed from the atmosphere, using absorption and electrodialysis. If the 4,940 TWh of excess electricity were utilised for DAC, it is estimated that 2.6 $MtCO_2$ could be captured annually, equating to about 6% of current UK emissions [11]. The International Energy Agency (IEA) estimates that to align with the Net Zero scenario, 80 $MtCO_2$ need to be captured from the atmosphere annually by 2030 [21]. Utilising global curtailed electricity for DAC could potentially meet 3.3% of this anticipated demand.

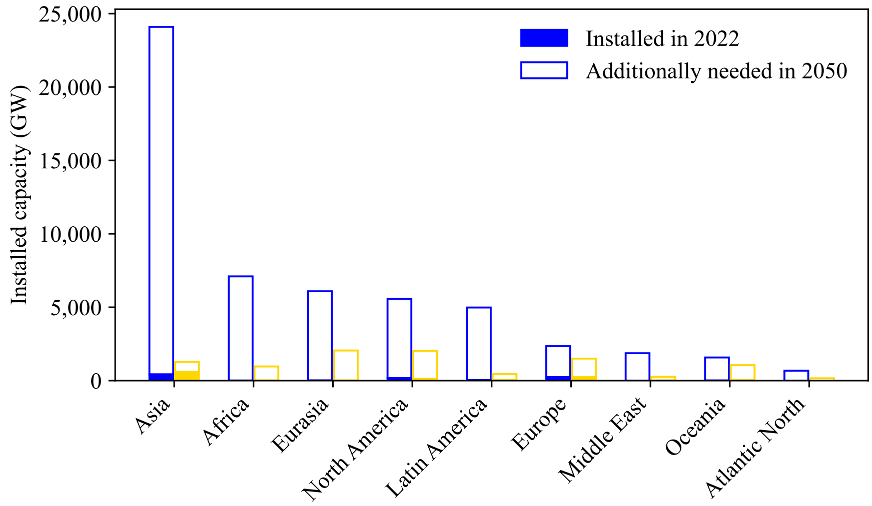

Figure 12: *Required wind (blue) and solar (yellow) capacity in 2050 compared to the installed capacity in 2022. Asia includes North Asia, South Asia, and South West Asia. Eurasia includes North West Asia and UPS [26, 27].*

Desalination is the process of removing salts and other impurities from seawater or brackish water to produce fresh water. On an industrial scale, reverse osmosis (RO) is the most commonly used method for this purpose. Using RO, the energy consumption can be as low as 2.5 kWh/m^3 [1]. If the 4,940 TWh of excess electricity were utilised for desalination, it is estimated that 1,976 km^3 of drinking water could be produced annually. To put this into perspective, global water demand is currently 4,600 km^3 per year and is expected to outstrip supply by 40% by 2030, increasing to as much as 6,000 km^3 per year by 2050 [8]. Utilising global curtailed electricity for desalination could potentially meet 33% of this anticipated demand.

4 Conclusion

This study investigated the energetic feasibility of a global electricity grid, powered entirely by wind and solar PV. The findings indicate that a global grid could maintain a continuous supply of renewable electricity sufficient to meet the projected demand throughout 2050.

Hourly time series predictions of electricity demand, as well as wind and solar potential, were obtained for each region. The power flow within the global grid was then simulated using PyPSA to determine the optimal global distribution of wind and solar PV capacities, aimed at minimising curtailment. A no transmission scenario was simulated where power flows were restricted, along with a transmission scenario where the resolution of the renewable energy potential was $4^\circ \times 4^\circ$. To evaluate the impact of the increased spatial resolution of renewable potential, a regional case in which the renewable potential was estimated as a spatial average across the entire region was also simulated.

In the transmission scenario, approximately 6.7% of global demand was lost during transmission, with time varying losses ranging between 5.9% and 8.7% of demand. The global grid relied primarily on wind energy in both the transmission and no transmission scenarios, with approximately 77% of generated electricity in the transmission scenario coming from wind and approximately 23% from solar PV. This suggests that wind generation better aligns with the daily demand curve, as it is not constrained by the solar cycle. These findings were shown to be insensitive to the choice of model parameters and the spatial resolution used to estimate renewable energy potential. Curtailment ranged from zero to 27.9% of generation, with a mean value of 7.9%. This mean value represents a reduction in curtailment of 92%, compared to the no transmission scenario.

An increase in the correlation coefficient between the time-varying global generation and global demand was observed, rising from 0.09 in the no transmission to 0.65 in the transmission scenario of the $4^\circ \times 4^\circ$ simulation. This indicates that a global grid significantly enhances the flexibility of a fully renewable electricity system. Furthermore, as the spatial resolution of renewable energy potential increased, a corresponding rise in the correlation coefficient was also observed. The maximum correlation of 0.65 occurred in the $4^\circ \times 4^\circ$ simulation, compared to only 0.08 in the regional case, where renewable potential was estimated as the spatial average across an entire region. This suggests that lower spatial resolutions capture intra-regional weather variability less effectively, limiting the system's ability to match generation with demand.

When examining global power flows in the transmission scenario, it was found that over 90% of global power flow is directed towards North Asia. North Asia accounts for nearly 40% of global electricity demand but generates less than one-third of what it needs, despite under utilising its potential wind and solar capacities, indicating that overall curtailment is reduced when North Asia imports surplus electricity rather than generating it itself. Additionally, a distinction between nodes acting as net importers, net exporters, and hubs could be observed, rather than regions alternately experiencing periods of electricity deficits and surpluses that complement each other. A frequency analysis of net flows highlighted temporal patterns in power flow activities, driven potentially by the solar cycle and human activity.

The power lost through transmission and curtailment were contextualised by comparing it to losses that would occur if other energy vectors (*e.g.*, hydrogen) were used or if the curtailed power were redirected for other purposes. The results obtained from the highest resolution simulation (*i.e.*, lowest curtailment) were used for this comparison. It was found that the efficiency of the global grid is significantly higher than that of hydrogen – 93.1% compared to approximately 30%. Additionally, if the excess electricity were used for hydrogen production, direct air capture (DAC), or desalination, it could address approximately 21.1% of the anticipated hydrogen demand in 2050, 3.3% of the global annual CO_2 removal required by 2030 to meet Net Zero targets, or meet 33% of the estimated global freshwater demand in 2050 through desalination.

Future studies should incorporate input data from various electricity demand projections and historical weather data from multiple years to mitigate the risks of over fitting. Consideration could then be given to exploring ways to enhance the flexibility (*i.e.*, the correlation between global generation and global demand) of wind and solar PV. One potential approach could involve clustering local wind and solar potentials into regions based on the linear independence of their capacity factors. Future research could also extend the analysis to consider region-specific land use availabilities to enhance the granularity of the results.

Acknowledgements

This research was supported by the National Research Foundation, Prime Minister's Office, Singapore under its Campus for Research Excellence and Technological Enterprise (CREATE) programme. For the purpose of open access, the author has applied a Creative Commons Attribution (CC BY) licence to any Author Accepted Manuscript version arising.

Declaration of Generative AI and AI-assisted technologies in the writing process

During the preparation of this work the authors used ChatGPT v4.0 in order to enhance the readability and language of the manuscript. After using this tool, the authors reviewed and edited the content as needed and take full responsibility for the content of the publication.

Data and code availability

All the codes developed, including the slightly modified version of GlobalEnergyGIS, are available in the GlobalGrid repository: https://github.com/cambridge-cares/GlobalGrid.

Conflicts of interest

There are no conflicts to declare.

A Appendix

A.1 Electricity grid model specification

Table A.1: *Overview of regions.*

No	Region	Coordinates (lat, lon)	Member countries
1	North America	(-106.5, 38.3)	Canada United States of America Mexico
2	Latin America	(-60.5, -13.3)	Argentina Bolivia Brazil Chile Colombia Cuba Dominican Rep. Ecuador Guatemala Haiti Honduras Paraguay Peru Puerto Rico Uruguay Venezuela Belize Costa Rica El Salvador Guyana Jamaica Nicaragua Panama Suriname Trinidad and Tobago
3	Oceania	(134.4, -22.6)	Australia New Zealand Cook Island Fiji Tonga Tuvalu Vanuatu New Caledonia Papua New Guinea Solomon Is.
4	North Asia	(116, 40.1)	China Hong Kong Japan Mongolia South Korea

No	Region	Coordinates (lat, lon)	Member countries
			Taiwan North Korea
5	South Asia	(114, 0.2)	Brunei Cambodia Indonesia Laos Malaysia Myanmar Philippines Singapore Thailand Timor-Leste Vietnam Maldives
6	North West Asia	(69.7, 48.6)	Afghanistan Azerbaijan Kazakhstan Kyrgyzstan Tajikistan Turkmenistan Uzbekistan Armenia Georgia Turkey
7	South West Asia	(74.2, 18.7)	Bangladesh Bhutan India Nepal Pakistan Sri Lanka
8	Middle East	(42.9, 29.7)	Bahrain Iran Iraq Israel Jordan Kuwait Lebanon Oman Qatar Saudi Arabia Syria United Arab Emirates Yemen Cyprus Palestine
9	Europe†	(10, 50)	Albania Austria Belgium Bosnia and Herz. Bulgaria

No	Region	Coordinates (lat, lon)	Member countries
			Croatia Czechia Denmark Estonia Finland France Germany Greece Hungary Ireland Italy Latvia Lithuania Luxembourg Malta Montenegro Netherlands N. Cyprus Norway Poland Portugal Romania Serbia Slovakia Slovenia Spain Sweden Switzerland United Kingdom Kosovo North Macedonia Moldova
10	Unified Power System (UPS)	(74, 66)	Belarus Russia Ukraine
11	North Africa	(-0.75, 27.5)	Algeria Egypt Libya Morocco Tunisia W. Sahara Sudan Somaliland
12	Africa	(21.6, -14)	Angola Benin Botswana Burkina Faso Burundi Cabo Verde Cameroon Central African Rep.

No	Region	Coordinates (lat, lon)	Member countries
			Côte d'Ivoire Chad Comoros Congo Dem. Rep. Congo Djibouti Eq. Guinea Eritrea eSwatini Ethiopia Gabon Gambia Ghana Guinea Guinea-Bissau Kenya Lesotho Liberia Madagascar Malawi Mali Mauritania Mozambique Namibia Niger Nigeria Rwanda São Tomé and Príncipe Senegal Seychelles Sierra Leone Somalia South Africa S. Sudan Tanzania Togo Uganda Zambia Zimbabwe
13	Atlantic North	(-45, 62)	Greenland Iceland

† The historic demand data are available for download from doi:10.17863/CAM.111494.

Table A.2: *Overview of interconnectors.*

No	Region 1	Region 2	Length (km)	Efficiency
1	North America	Latin America	7,454	0.89
2	North America	UPS	8,440	0.88
3	North America	Atlantic North	4,869	0.92
4	Oceania	South Asia	3,354	0.94
5	North Asia	South Asia	4,423	0.93
6	North Asia	North West Asia	3,749	0.94
7	North Asia	South West Asia	4,640	0.93
8	North Asia	UPS	3,894	0.94
9	South Asia	South West Asia	4,805	0.92
10	North West Asia	South West Asia	3,341	0.94
11	North West Asia	Middle East	3,096	0.95
12	North West Asia	UPS	1,954	0.96
13	Middle East	Europe	3,558	0.94
14	Middle East	UPS	4,557	0.93
15	Middle East	North Africa	4,251	0.93
16	Middle East	Africa	5,349	0.92
17	Europe	UPS	3,956	0.93
18	Europe	North Africa	2,660	0.95
19	Europe	Atlantic North	3,552	0.94
20	North Africa	Africa	5,187	0.92

Table A.3: *Coordinate reference systems (CRS) by region.*

Region	Code
Atlantic North	32629
Africa	4326
North Africa	32634
UPS	3413
South West Asia	32638
North West Asia	32642
South Asia	32643
North Asia	32645
Latin America	4326
Europe	3035
North America	5070
Middle East	32637
Oceania	3577

A.2 Demand multipliers

Table A.4: *Demand multiplier for the SSP1 scenarios for Latin America (LAM), OECD countries, ASIA, Middle East and Africa (MAF), and reforming economies (REF) [22].*

Scenario	LAM	OECD	Asia	MAF	REF
ssp1-19	2.74	1.35	2.48	3.96	1.36
ssp1-26	2.53	1.36	2.51	3.67	1.43
ssp1-34	2.64	1.36	2.64	3.85	1.50
ssp1-45	2.67	1.37	2.73	3.97	1.59

A.3 Power losses

Power losses occur during the transmission and distribution of electrical energy due to the inherent resistance and impedance of transmission lines and equipment. These losses can be categorised into converter station losses and transmission line losses.

Converter losses occur during the conversion from AC to DC and vice versa and typically range from 0.5% to 1% of the rated power [10].

Transmission losses can be further segmented into ohmic losses and corona losses. The losses are typically expressed in the units of kW/km. Ohmic losses occur because resistance to the flow produces heat (thermal energy) which is dissipated to the surroundings and can be expressed as

$$L_{\mathrm{R}} = I^2 R, \tag{A.1}$$

where L_{R} are the ohmic (*i.e.*, resistive) losses, I is current, and R the resistance. Since DC current can also be expressed as $I = \frac{P}{V}$, where P is the power and V is the voltage, ohmic losses can be calculated as a relative value for each transmission line given the rated power, voltage, resistivity, and length, L:

$$L_{\mathrm{R}} = \left(\frac{P}{V}\right)^2 RL. \tag{A.2}$$

Table A.5: *Technical specifications of an advanced UHVDC cable [10, 17].*

	UHVDC
Cable voltage	$\pm 1,100$ kV
Power capacity	1.2 GW
Conductor resistivity	0.01286 Ω/km

A.4 Additional results

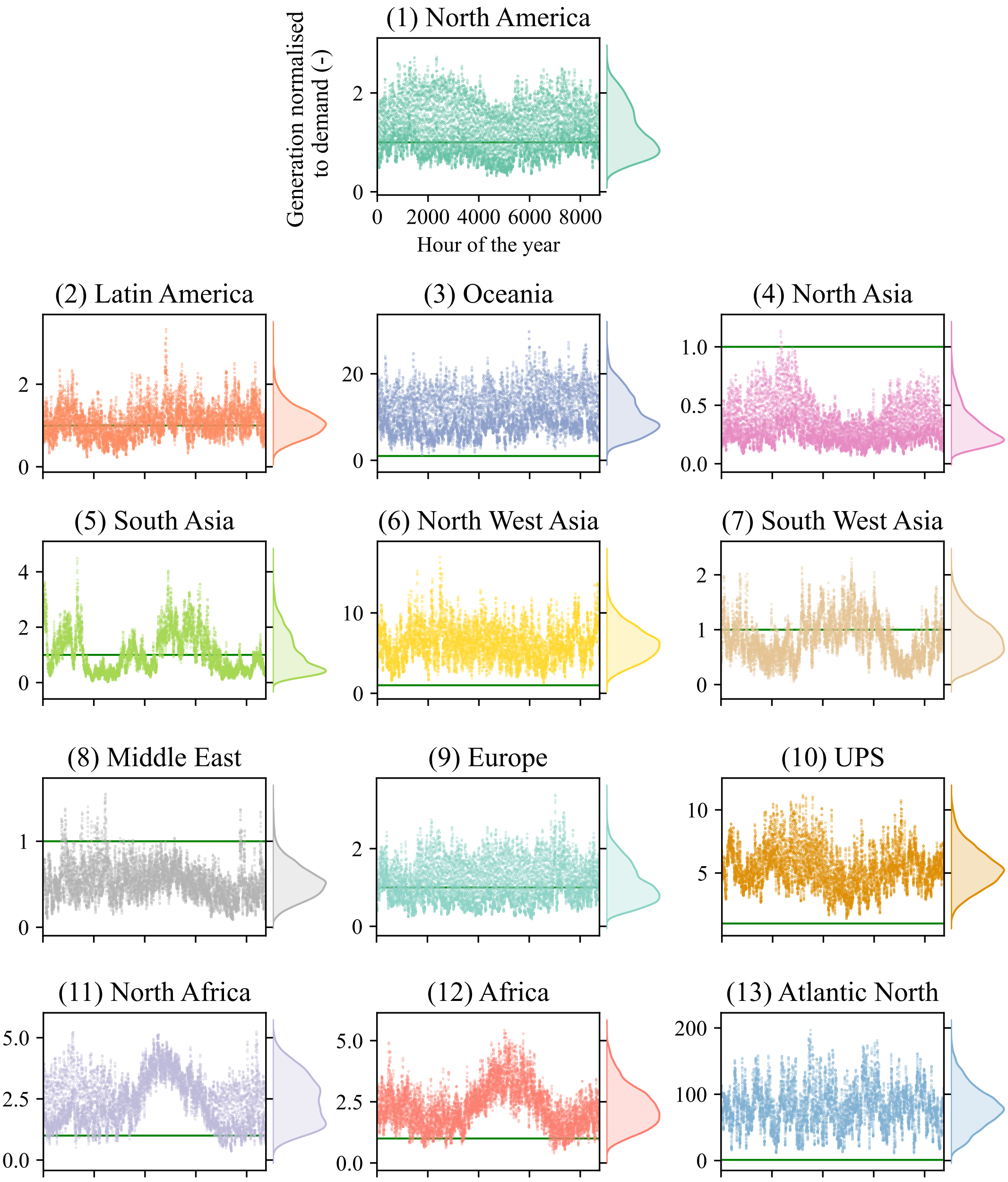

Figure A.1: *Generation normalised to demand. Each dot represents one hour of the year.*

	North America	Latin America	Oceania	North Asia	South Asia	North West Asia	South West Asia	Middle East	Europe	Ups	North Africa	Africa	Atlantic North
North America	0.02	0.00	0.04	0.09	0.04	0.03	0.14	0.08	0.11	0.02	0.08	0.05	0.02
Latin America	0.00	0.00	0.02	0.12	0.00	0.00	0.07	0.01	0.24	0.00	0.13	0.18	0.00
Oceania	0.04	0.02	0.04	0.03	0.00	0.04	0.13	0.06	0.18	0.00	0.08	0.17	0.03
North Asia	0.09	0.12	0.03	0.00	0.07	0.02	0.14	0.13	0.02	0.00	0.01	0.06	0.00
South Asia	0.04	0.00	0.00	0.07	0.00	0.00	0.08	0.04	0.23	0.22	0.21	0.28	0.00
North West Asia	0.03	0.00	0.04	0.02	0.00	0.00	0.10	0.03	0.21	0.10	0.03	0.24	0.00
South West Asia	0.14	0.07	0.13	0.14	0.08	0.10	0.11	0.25	0.46	0.32	0.46	0.36	0.11
Middle East	0.08	0.01	0.06	0.13	0.04	0.03	0.25	0.04	0.20	0.13	0.09	0.06	0.04
Europe	0.11	0.24	0.18	0.02	0.23	0.21	0.46	0.20	0.18	0.20	0.22	0.32	0.20
Ups	0.02	0.00	0.00	0.00	0.22	0.10	0.32	0.13	0.20	0.00	0.00	0.09	0.09
North Africa	0.08	0.13	0.08	0.01	0.21	0.03	0.46	0.09	0.22	0.00	0.01	0.13	0.01
Africa	0.05	0.18	0.17	0.06	0.28	0.24	0.36	0.06	0.32	0.09	0.13	0.20	0.19
Atlantic North	0.02	0.00	0.03	0.00	0.00	0.00	0.11	0.04	0.20	0.09	0.01	0.19	0.12

Figure A.2: *R^2 matrix where the independent variables are the wind and solar capacity factors of two regions and the dependent variable are the sum of their electricity demand profiles.*

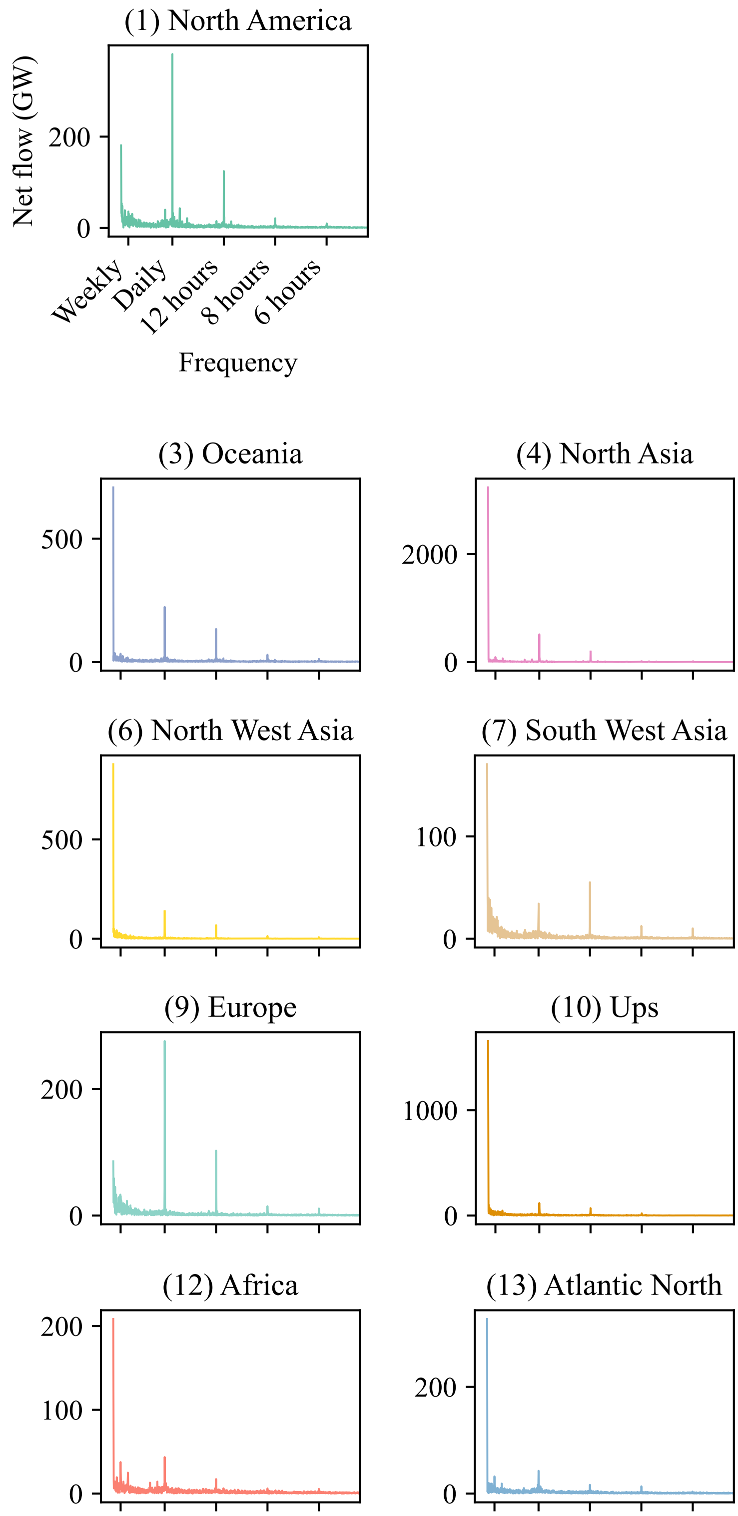

Figure A.3: *Fourier transform of the hourly net flow through each region. Each panel uses its own scale for the net flow axis.*

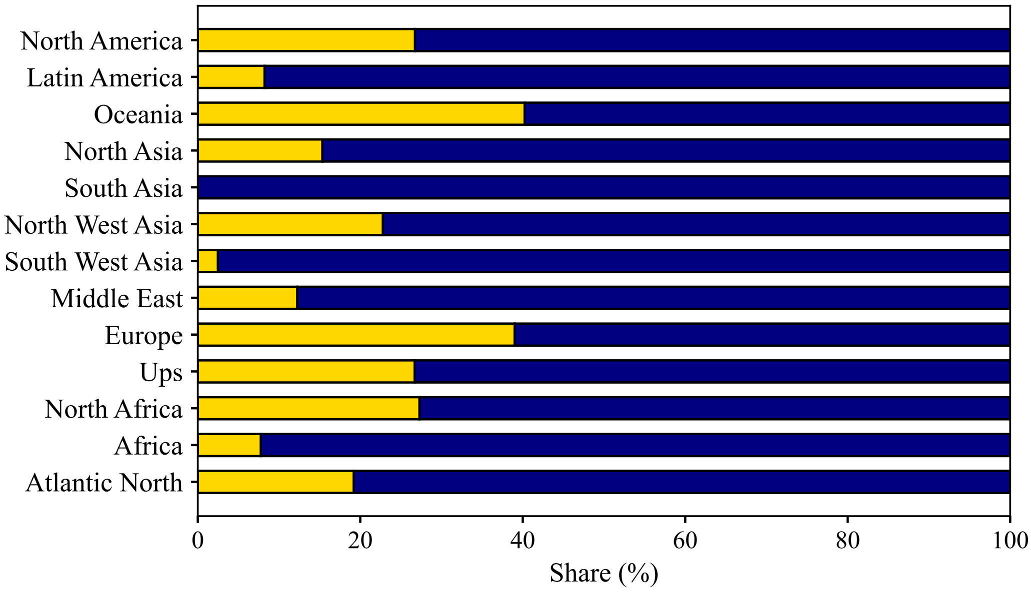

Figure A.4: *Regional shares of installed wind (blue) and solar (yellow) capacity.*

Table A.6: *Wind and solar PV land use (% of total land area) and share of installed capacity (%) for each region in the no transmission and transmission scenario.*

	No transmission scenario				**Transmission scenario**			
	Land use		**Installed capacity**		**Land use**		**Installed capacity**	
Region	**Wind**	**Solar**	**Wind**	**Solar**	**Wind**	**Solar**	**Wind**	**Solar**
North America	3.24	0.09	89.08	10.92	2.59	0.21	73.26	26.74
Latin America	4.67	0.03	97.12	2.88	2.69	0.05	91.78	8.22
Oceania	0.43	0.02	83.64	16.36	1.86	0.28	59.77	40.23
North Asia	28.25	0.23	96.47	3.53	2.45	0.10	84.66	15.34
South Asia	82.33	0.16	99.14	0.86	17.40	0.00	100.00	0.00
North West Asia	2.03	0.03	93.82	6.18	3.67	0.24	77.21	22.79
South West Asia	55.93	0.28	97.83	2.17	10.82	0.06	97.52	2.48
Middle East	14.47	0.35	90.21	9.79	3.61	0.11	87.75	12.25
Europe	13.91	0.61	83.56	16.44	4.55	0.65	60.99	39.01
UPS	0.58	0.04	77.85	22.15	1.44	0.12	73.31	26.69
North Africa	1.23	0.07	79.22	20.78	1.62	0.13	72.71	27.29
Africa	0.95	0.03	88.77	11.23	2.64	0.05	92.23	7.77
Atlantic North	0.07	0.00	84.74	15.26	2.93	0.15	80.80	19.20

A.5 Sensitivity to parameter choices

The results in the following section assess the sensitivity of the results to the parameter choices versus a "base scenario" based on the results presented in the main text.

Figure A.5 shows the influence of the CapEx and OpEx on the system behaviour. It can be seen that when the ratio between capacity cost and generation cost exceeds 100:1 (MWh/MW), both annual global generation and transmission begin to increase. This behaviour arises because high capacity costs discourage the deployment of new capacity, shifting the optimisation focus toward minimising installed capacity rather than reducing excess electricity generation. Conversely, when the cost of electricity generation is set to zero, the optimisation algorithm seeks a solution that minimises the sharp spikes in the regional generation curve – these correlate with the deployed capacities in each region. In contrast, when capacity costs are set to zero, the algorithm focuses on minimising the total area under the global generation curve, leading to a different optimisation pathway.

Figure A.6 illustrates the influence of the weights assigned to wind and solar capacity deployment, as well as electricity generation, on system behaviour. The optimal point is observed when the ratio of these weights is equal to one, as this minimises total generation. This outcome is intuitive because, when the deployment or generation costs of wind and solar are not balanced, the system tends to stimulate demand by favouring the deployment of the "cheaper" generation option – even if it is less aligned with the demand curve. This is further demonstrated in the graph at the top right of **Figure** A.6, which shows that higher wind costs lead to a reduced share of wind in the generation mix, and vice versa. At the bottom left of **Figure** A.6 it can be seen that, unlike annual generation, annual transmission decreases when wind costs are higher than solar costs and increases when solar costs are higher than wind costs. This behaviour can be attributed to the solar cycle. When wind costs are higher, the system heavily relies on deploying solar capacity. However, since solar PV generation is minimal during the night due to the absence of sunlight, the system compensates by importing solar energy from other regions rather than deploying wind capacity to meet demand during these periods.

Figure A.7 illustrates the impact of varying transmission costs relative to generation costs on the system. It is evident that power flow decreases significantly when transmission costs exceed generation costs. This outcome aligns with expectations, as the optimisation favours generating additional energy at the demand node over transmitting electricity from other locations. The system appears to converge at a generation-to-transmission cost ratio of 10:1 (MWh/MWh). Since only a small cost is assigned to transmission to resolve potential degeneracies in the linear programming model, the system is considered largely insensitive to changes in this parameter.

Figure A.8 illustrates the sensitivity of the system to changes in land use availability. The results demonstrate that annual generation and transmission converge at the land use availabilities chosen for the simulation, indicating that the selected values do not constrain the system. However, when land use availabilities are reduced, some regions reach their maximum allowable capacity. This necessitates importing less efficient electricity from other regions, which in turn increases both transmission and generation requirements. Future research could explore region-specific land use availabilities to enhance the granularity of the results.

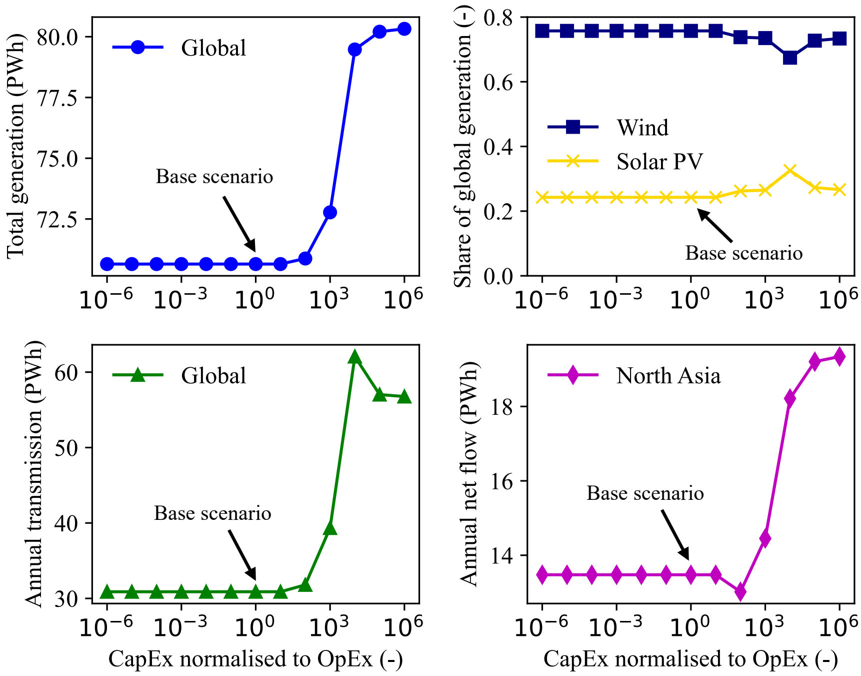

Figure A.5: *Sensitivity analysis of CapEx vs OpEx.*

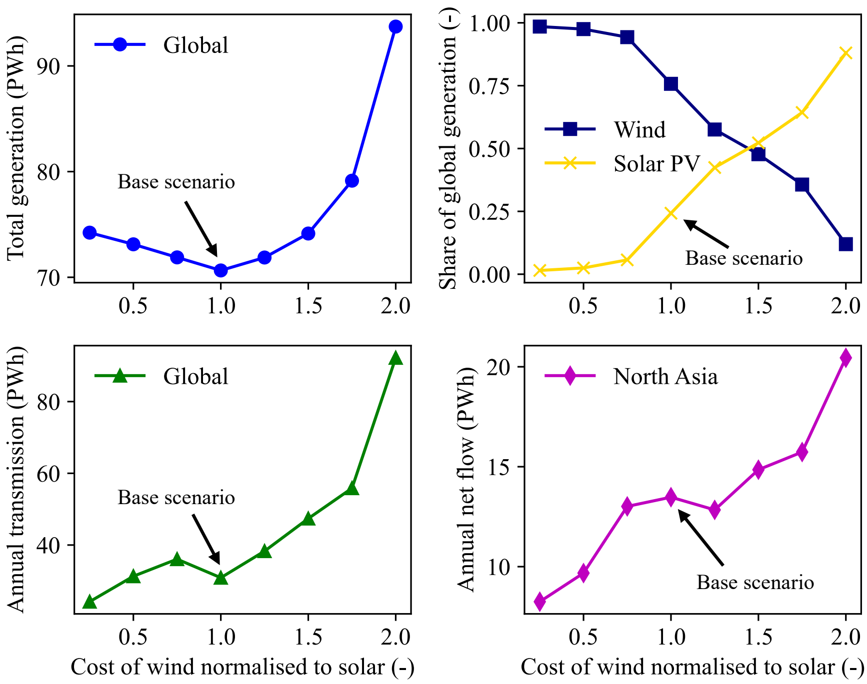

Figure A.6: *Sensitivity analysis of wind cost vs solar cost.*

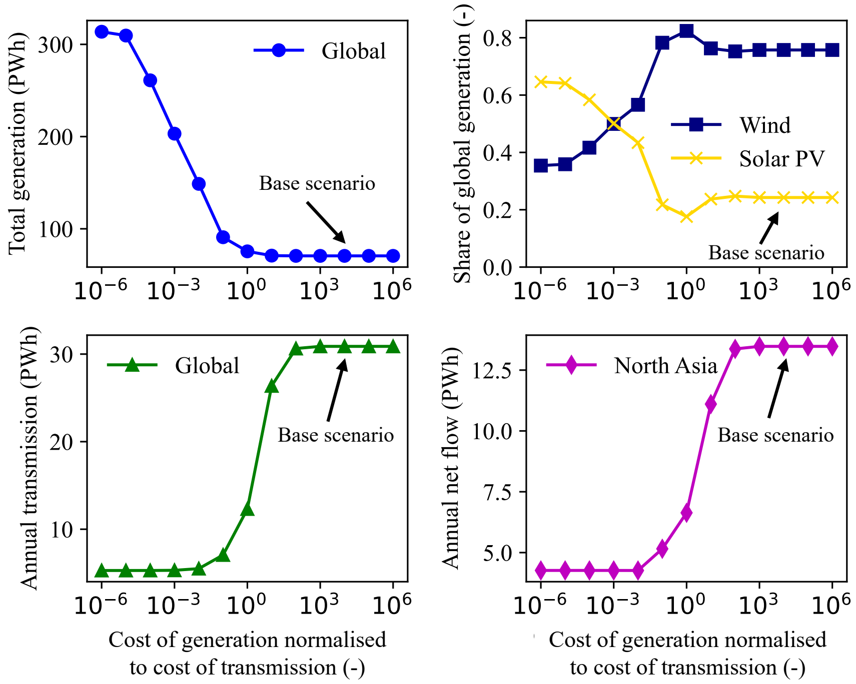

Figure A.7: *Sensitivity analysis of transmission cost vs generation cost.*

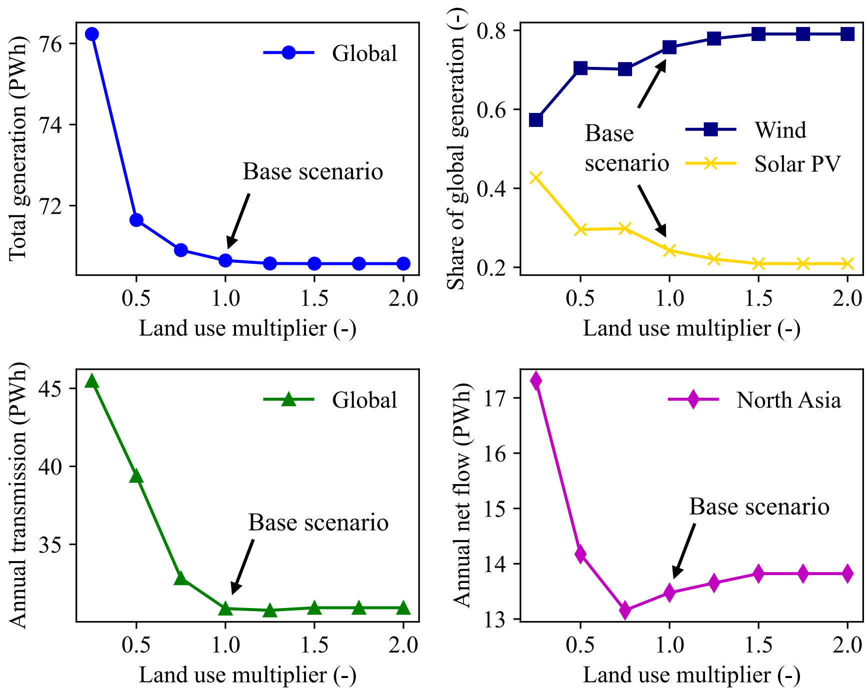

Figure A.8: *Sensitivity analysis of land use availability: The land use availabilities for wind and solar were scaled by the factor indicated on the horizontal axis.*

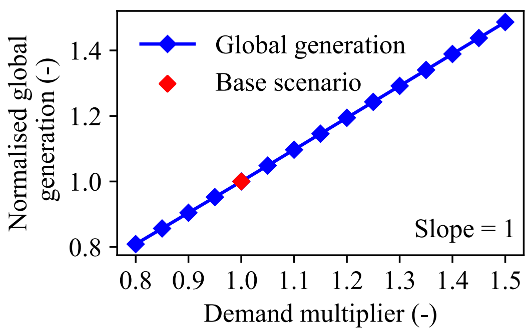

Figure A.9: *Variations in total global energy generation in response to uniform changes in global energy demand. The generation is normalised to the base scenario.*

References

[1] AMTA. America's authority in membrane treatment membrane desalination power usage put in perspective, 2016. URL https://www.amtaorg.com/wp-content/uploads/07_Membrane_Desalination_Power_Usage_Put_In_Perspective.pdf. Accessed August 2024.

[2] M. Ardelean. Optimal paths for electricity interconnections between Central Asia and Europe. Technical report, Joint Research Centre, 2020.

[3] M. Ardelean and P. Minnebo. A China-EU electricity transmission link Assessment of potential connecting countries and routes. Technical report, Joint Research Centre, 2018.

[4] J. Atherton, W. Xie, F. Farazi, S. Mosbach, J. Akroyd, and M. Kraft. Breakdown of British wind curtailment using a multi-source knowledge graph approach, 2023. URL https://como.ceb.cam.ac.uk/. Accessed July 2024.

[5] Australian Government. Australia-Asia PowerLink - Business case evaluation summary, 2022. URL https://www.infrastructureaustralia.gov.au/sites/default/files/2022-06/Evaluation%20Summary%20-%20Australia-Asia%20PowerLink.pdf. Accessed August 2024.

[6] L. Bauer and S. Matysik. Vestas V112-3.075 onshore – 3,08 mw – wind turbine, 2024. URL https://en.wind-turbine-models.com/turbines/7-vestas-v112-3.075-onshore. Accessed July 2024.

[7] D. Bogdanov and C. Breyer. North-east Asian super grid for 100*Energy Conversion and Management*, 112:176–190, 2016. doi:10.1016/J.ENCONMAN.2016.01.019.

[8] A. Boretti and L. Rosa. Reassessing the projections of the world water development report. *npj Clean Water 2019 2:1*, 2:1–6, 7 2019. doi:10.1038/s41545-019-0039-9.

[9] P. R. Brown and A. Botterud. The value of inter-regional coordination and transmission in decarbonizing the US electricity system. *Joule*, 5:115–134, 2021. doi:10.1016/J.JOULE.2020.11.013.

[10] Z. Chen, C. Wang, J. Li, F. Song, and Z. Zhang. Conductor selection and economic analysis of D.R. Congo–Guinea ±800 kv UHVDC transmission project. *Global Energy Interconnection*, 3:385–397, 2020. doi:10.1016/J.GLOEI.2020.10.007.

[11] Department for Energy Security and Net Zero. 2020 UK greenhouse gas emissions, 2022. URL https://assets.publishing.service.gov.uk/media/61f7fb418fa8f5389450212e/2020-final-greenhouse-gas-emissions-statistical-release.pdf. Accessed August 2024.

[12] EuroAfrica Interconnector. Euroafrica construction, 2021. URL https://www.euroafrica-interconnector.com/cable-construction/. Accessed July 2024.

[13] A. Franco and C. Giovannini. Recent and future advances in water electrolysis for green hydrogen generation: Critical analysis and perspectives. *Sustainability 2023, Vol. 15, Page 16917*, 15:16917, 12 2023. doi:10.3390/SU152416917.

[14] Geopandas. Geopandas 1.0.1, 2013. URL https://geopandas.org/en/stable/. Accessed August 2024.

[15] S. Giddey. Ammonia as a renewable energy transportation media. *ACS Sustainable Chemistry and Engineering*, 5:10231–10239, 11 2017. doi:10.1021/ACSSUSCHEMENG.7B02219.

[16] C. Gulli. Global energy perspective 2023: Hydrogen outlook | mckinsey, 2024. URL https://www.mckinsey.com/industries/oil-and-gas/our-insights/global-energy-perspective-2023-hydrogen-outlook. Accessed July 2024.

[17] Hitachi China. Changji-Guquan UHVDC link, 2024. URL https://www.hitachienergy.com/uk-ie/en/about-us/customer-success-stories/changji-guquan-uhvdc-link. Accessed July 2024.

[18] F. Hofmann, J. Hampp, F. Neumann, T. Brown, and J. Hörsch. atlite: A lightweight python package for calculating renewable power potentials and time series. *Journal of Open Source Software*, 6:3294, 6 2021. doi:10.21105/JOSS.03294.

[19] IEA. Greenhouse gas emissions from energy data explorer – data tools, 2023. URL https://www.iea.org/data-and-statistics/data-tools/greenhouse-gas-emissions-from-energy-data-explorer. Accessed July 2024.

[20] IEA. Executive summary – renewables 2023 – analysis - iea, 2024. URL https://www.iea.org/reports/renewables-2023/executive-summary#. Accessed July 2024.

[21] IEA. Direct air capture - energy system - iea, 2024. URL https://www.iea.org/energy-system/carbon-capture-utilisation-and-storage/direct-air-capture. Accessed July 2024.

[22] N. Mattsson, V. Verendel, F. Hedenus, and L. Reichenberg. An autopilot for energy models – automatic generation of renewable supply curves, hourly capacity factors and hourly synthetic electricity demand for arbitrary world regions, 3 2020. URL https://arxiv.org/abs/2003.01233v1. Accessed July 2024.

[23] A. Purvins, L. Sereno, M. Ardelean, C.-F. Covrig, T. Efthimiadis, and P. Minnebo. Submarine power cable between Europe and North America: A techno-economic analysis. *Journal of Cleaner Production*, 186:131–145, 6 2018. doi:10.1016/J.JCLEPRO.2018.03.095.

[24] L. Reichenberg, F. Hedenus, N. Mattsson, and V. Verendel. Deep decarbonization and the supergrid – Prospects for electricity transmission between Europe and China. *Energy*, 239:122335, 2022. doi:10.1016/j.energy.2021.122335.

[25] K. Riahi, D. P. van Vuuren, E. Kriegler, J. Edmonds, B. C. O'Neill, S. Fujimori, N. Bauer, K. Calvin, R. Dellink, O. Fricko, W. Lutz, A. Popp, J. C. Cuaresma, S. KC, M. Leimbach, L. Jiang, T. Kram, S. Rao, J. Emmerling, K. Ebi, T. Hasegawa, P. Havlik, F. Humpenöder, L. A. D. Silva, S. Smith, E. Stehfest, V. Bosetti, J. Eom, D. Gernaat, T. Masui, J. Rogelj, J. Strefler, L. Drouet, V. Krey, G. Luderer, M. Harmsen, K. Takahashi, L. Baumstark, J. C. Doelman, M. Kainuma, Z. Klimont, G. Marangoni, H. Lotze-Campen, M. Obersteiner, A. Tabeau, and M. Tavoni. The shared socioeconomic pathways and their energy, land use, and greenhouse gas emissions implications: An overview. *Global Environmental Change*, 42:153–168, 1 2017. doi:10.1016/J.GLOENVCHA.2016.05.009.

[26] P. Rosado, M. Roser, and H. Ritchie. Installed solar energy capacity, 2023. URL https://ourworldindata.org/grapher/installed-solar-pv-capacity?country=OWID_WRL~OWID_AFR~OWID_EUR~Africa+%28IRENA%29~Asia+%28IRENA%29~Central+America+and+the+Caribbean+%28IRENA%29~Europe+%28IRENA%29~Middle+East+%28IRENA%29~North+America+%28IRENA%29~Oceania+%28IRENA%29~South+America+%28IRENA%29~Eurasia+%28IRENA%29#reuse-this-work. Accessed July 2024.

[27] P. Rosado, M. Roser, and H. Ritchie. Installed wind energy capacity, 2023. URL https://ourworldindata.org/grapher/cumulative-installed-wind-energy-capacity-gigawatts?country=Europe+%28IRENA%29~Oceania+%28IRENA%29~South+America+%28IRENA%29~Africa+%28IRENA%29~Asia+%28IRENA%29~Eurasia+%28IRENA%29~Middle+East+%28IRENA%29~North+America+%28IRENA%29~Central+America+and+the+Caribbean+%28IRENA%29~OWID_WRL~ISL~GRL. Accessed July 2024.

[28] United Nations. Net zero coalition, 2024. URL https://www.un.org/en/climatechange/net-zero-coalition. Accessed June 2024.

[29] P. Viebahn, A. Scholz, and O. Zelt. The potential role of direct air capture in the german energy research program—results of a multi-dimensional analysis. *Energies 2019, Vol. 12, Page 3443*, 12:3443, 9 2019. doi:10.3390/EN12183443.

[30] J. Whitaker. pyproj 3.6.1, 2024. URL https://pypi.org/project/pyproj/. Accessed August 2024.

[31] C. Wu, X. P. Zhang, and M. J. Sterling. Global electricity interconnection with 100% renewable energy generation. *IEEE Access*, 9:113169–113186, 2021. doi:10.1109/ACCESS.2021.3104167.

[32] Xlinks. Xlinks capturing and connecting the power of nature, 2024. URL https://xlinks.co/. Accessed July 2024.

[33] J. Yu, K. Bakic, A. Kumar, A. Iliceto, L. Beleke Tabu, J. Ruaud, J. Fan, B. Cova, H. Li, D. Ernst, R. Fonteneau, M. Theku, G. Sanchis, M. Chamollet, M. Le Du, Y. Zhang, S. Chatzivasileiadis, D.-C. Radu, M. Berger, M. Stabile, F. Heymann, M. Dupré La Tour, M. Manuel de Villena Millan, and M. Ranjbar. Global electricity network - feasibility study. Technical report, CIGRE, 2019. URL https://orbi.uliege.be/handle/2268/239969. Accessed July 2024.

[34] W. Zappa, M. Junginger, and M. van den Broek. Is a 100% renewable European power system feasible by 2050? *Applied Energy*, 233-234:1027–1050, 2019. doi:10.1016/J.APENERGY.2018.08.109.